JOC Article

Insights on Co-Catalyst-Promoted Enamine Formation between Dimethylamine and Propanal through Ab Initio and Density Functional Theory Study

Mahendra P. Patil and Raghavan B. Sunoj*

Department of Chemistry, Indian Institute of Technology Bombay, Powai, Mumbai 400076, India

sunoj@chem.iitb.ac.in

Received May 11, 2007

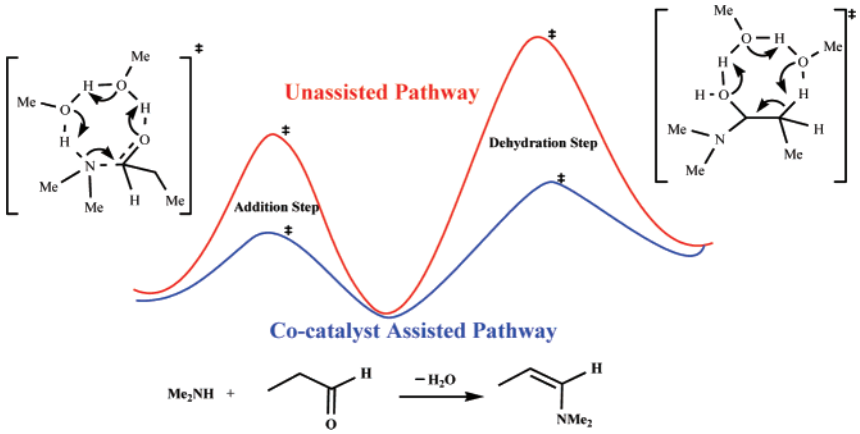

The mechanistic details on enamine formation between dimethylamine and propanal are unraveled using the ab initio and density functional theory methods. The addition of secondary amine to the electrophile and simultaneous proton transfer results in a carbinolamine intermediate, which subsequently undergoes dehydration to form enamine. The direct addition of amine as well as the dehydration of the resulting carbinolamine intermediate is predicted to possess fairly high activation barrier implying that a unimolecular process is unlikely to be responsible for enamine formation. Different models are therefore proposed which could explain the relative ease of enamine formation under neat condition as well as under the influence of methanol as the co-catalyst. The explicit inclusion of either the reagent or the co-catalyst is considered in the transition states as stabilizing agents. The participation of the reagent or the co-catalyst as a monofunctional ancillary species is found to stabilize the transition states relative to the unassisted or the direct addition/dehydration pathways. The reduction in enthalpy of activation is found to be much more dramatic when two co-catalysts participate in an active bifunctional mode in the rate-determining dehydration step. The transition structures exhibited characteristic features of a relay proton transfer mechanism. The free energy of activation associated with the two methanol-assisted pathway is found to be 16.7 kcal/mol lower than that of the unassisted pathway. The results are found to be in concurrence with the available reports on the rate acceleration by co-catalysts in the Michael reaction between enamine and methyl vinyl ketone under neat conditions.

Introduction

The importance of enamines as useful nucleophiles in the carbon−carbon bond forming reaction has been growing enormously ever since the seminal studies reported by Stork and co-workers.[1] Nucleophilic reactivity of the β-carbon in enamines makes them attractive building blocks in organic synthesis.[2,3] The role of enamine intermediates in several biological processes is also well-known.[4,5] Enamine catalysis has been identified as a simple protocol in rendering improved reactivities for keto compounds in nucleophilic addition reac-

(1) (a) Stork, G.; Terrell, R.; Szmuszkovicz, J. *J. Am. Chem. Soc.* **1954**, *76*, 2029. (b) Stork, G.; Brizzolona, A.; Landesman, H.; Szmuszkovicz, J.; Terrell, R. *J. Am. Chem. Soc.* **1963**, *85*, 207.

10.1021/jo071004q CCC: $37.00
Published on Web 09/27/2007

SCHEME 1. Two Key Steps (Addition and Dehydration) toward the Formation of Enamine from Dimethylamine and Propanal

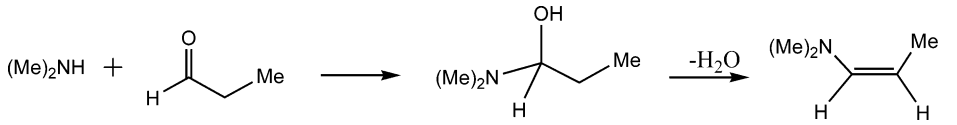

Step-I: Carbinolamine Formation Step-II: Enamine Formation

tions.[6] Recent surge of activities in asymmetric organocatalysis, most of which are proposed to proceed through enamine intermediates, has set the stage for renewed attention on the mechanistic features of enamine-mediated reactions.[7] In recent years, special reaction conditions, such as ionic liquids and surfactants, have also been employed for organocatalytic reactions.[8] While polar organic solvents are commonly used,[9] an increasing number of reports is now available on organocatalytic reactions in aqueous medium.[10] These recent studies conspicuously highlight the importance of understanding the role of reaction media on enamine formation as well as its reactions.

There have been a number of experimental as well as theoretical investigations on the mechanism of formation of iminium/enamine.[11] The rate of enamine formation is largely governed by either of the two steps, namely, the formation of carbinolamine intermediate or the subsequent dehydration leading to enamine (Scheme 1). Acid−base-catalyzed enamine formation is fairly well understood through the kinetic studies of Sayer and co-workers.[11a−c] The semiempirical as well as ab initio theoretical studies reported, respectively, by William[12a] and later by Smith and co-workers were able to shed light on the role of explicit solvent (water) molecules on the reaction energetics.[12d]A simple bimolecular reaction between methylamine and formaldehyde has been estimated to possess a barrier as high as 26.7 and 55.3 kcal mol^{-1}, respectively, for the carbinolamine formation and subsequent dehydration leading to imine at the G2(MP2,SVP) level of theory.[12d] Water molecule has been found to be effective in catalyzing both the steps through explicit stabilization of the corresponding transition states. It is worth noting that several organocatalytic reactions involving enamines are carried out either under neat conditions or in aprotic solvents.[13] Considering the higher barriers for addition as well as dehydration steps, it is reasonable to envisage that the enamine formation could perhaps be catalyzed by other available reagents in the reaction mixture. These include in situ generated water and[14] reagents such as amine, aldehyde, or an added co-catalyst. The kinetic assistance provided in the form

(2) Reviews on enamine chemistry: (a) Hickmott, P. W. *Tetrahedron* **1982**, *38*, 1975. (b) d'Angelo, J.; Desmaële, D.; Dumas, F.; Guingant, A.; *Tetrahedron: Asymmetry* **1992**, *3*, 459.

(3) (a) List, B. *Acc. Chem. Res.* **2004**, *37*, 548. (b) Carey F. A.; Sundberg, R. J. *Advanced Organic Chemistry; Part B: Reaction and Synthesis*; Kluwer Academic: New York.

(4) (a) Wang, C.-H.; Whitesides, G. M. *Enzymes in Synthetic Organic Chemistry*; Pergamon: Oxford, 1994.

(5) (a) Lai, C. Y.; Nakai, N.; Chang, D. *Science* **1974**, *183*, 1204. (b) Morris, A. J.; Tolan, D. R. *Biochemistry* **1994**, *33*, 12291. (c) Wagner, J.; Lerner, R. A.; Barbas, C. F., III. *Science* **1995**, *270*, 1797. (d) Barbas, C. F., III; Heine, A.; Zhong, G.; Hoffmann, T.; Grammatikova, S.; Björnestedt, R.; List, B.; Anderson, J.; Stura, E. A.; Wilson, I. A.; Lerner, R. A. *Science* **1997**, 278, 2085. (e) Choi, K. H.; Shi, J.; Hopkins, C. E.; Tolan, D. R.; Allen, K. N. *Biochemistry* **2001**, *40*, 13868. (f) Heine, A.; DeSantis, G.; Luz, J. G.; Mitchell, M.; Wong, C.-H.; Wilson, I. A. *Science* **2001**, *294*, 369.

(6) Notz, W.; Tanaka, F.; Barbas, C. F., III. *Acc. Chem. Res*. **2004**, *37*, 590. (b) Allemann, C.; Gordillo, R.; Clemente, F. R.; Cheong, P. H.-Y.; Houk, K. N. *Acc. Chem. Res*. **2004**, *37*, 558.

(7) Review on organocatalysis: (a) Dalko, P. I.; Moison, I. *Angew. Chem., Int. Ed*. **2001**, *40*, 3726. (b) List, B. *Tetrahedron* **2002**, *58*, 5573. (c) Dalko, P. I.; Moison, I. *Angew. Chem., Int. Ed*. **2004**, *43*, 5138. (d) List, B. *Chem. Commun*. **2006**, 819.

(8) (a) Chowdari, N. S.; Ramachary, D. B.; Barbas, C. F., III. *Synlett* **2003**, 1906. (b) Kotrusz, P.; Alemayehu, S.; Toma, S.; Schmalz, H.-G.; Alder, A. *Eur. J. Org. Chem*. **2005**, 4904. (c) Xu, L.-W.; Gao, Y.; Yin, J.-J.; Li, L.; Xia, C.-G. *Tetrahedron Lett.* **2005**, *46*, 5317. (d) Hayashi, Y.; Aratake, S.; Okano, T.; Takahashi, J.; Sumiya, T.; Shoji, M. *Angew. Chem., Int. Ed*. **2006**, *45*, 5527. (e) Luo, S.; Mi, X.; Zhang, L.; Liu, S.; Xu, H.; Cheng, J.-P. *Angew. Chem., Int. Ed*. **2006**, *45*, 3093. (f) Luo, S.; Mi, X.; Liu, S.; Xu, H.; Cheng, J.-P. *Chem. Commun*. **2006**, 3687. (g) Huang, K.; Huang, Z.; Li, X. *J. Org. Chem*. **2006**, *71*, 8320.

(9) (a) Page, P. C. B.; Barros, D.; Buckley, B. R.; Ardakani, A.; Marples, B. A. *J. Org. Chem*. **2004**, *69*, 3595. (b) Suri, J. T.; Steiner, D. D.; Barbas, C. F., III. *Org. Lett*. **2005**, *7*, 3885. (c) Dambruoso, P.; Massi, A.; Dondoni, A. *Org. Lett*. **2005**, *7*, 4657. (d) Fustero, S.; Jimenez, D.; Sanz-Cervera, J. F.; Sanchez-Rosello, M.; Esteban, E.; Simon-Fuentes, A. *Org. Lett*. **2005**, *7*, 3433. (e) Wang, W.; Wang, J.; Li, H. *Angew. Chem., Int. Ed.* **2005**, *44*, 1369. (f) Brandau, S.; Landa, A.; Franzeìn, J.; Marigo, M.; Jørgensen, K. A. *Angew. Chem., Int. Ed*. **2006**, *45*, 4305. (g) Coìrdova, A.; Zou, W.; Dziedzic, P.; Ibrahem, I.; Reyes, E.; Xu, Y. *Chem.—Eur. J*. **2006**, *12*, 5383. (h) Wang, J.; Li, H.; Lou, B.; Zu, L.; Guo, H.; Wang, W. *Chem.—Eur. J*. **2006**, *12*, 4321. (i) Grondal, C.; Enders, D. *Tetrahedron* **2006**, *62*, 329.

(10) (a) Northrup, A. B.; MacMillan, D. W. C. *J. Am. Chem. Soc*, **2002**, *124*, 2458. (b) Coìrdova, A.; Barbas, C. F., III. *Tetrahedron Lett.* **2003**, *44*, 1923. (c) Dickerson, T. J.; Lovell, T.; Meijler, M. M.; Noodleman, L.; Janda, K. M. *J. Org. Chem*. **2004**, *69*, 6603. (d) Lemay, M.; Ogilvie, W. W. *Org. Lett*. **2005**, *7*, 4141. (e) Rogers, C. J.; Dickerson, T. J.; Brogan, A. P.; Janda, K. D. *J. Org. Chem*. **2005**, *70*, 3705. (f) Jiang, Z.; Liang, Z.; Wu, X.; Lu, Y. *Chem. Commun*. **2006**, 2801. (g) Zu, L.; Wang, J.; Li, H.; Wang, W. *Org. Lett*. **2006**, *8*, 3077. (h) Hayashi, Y.; Sumiya, T.; Takahashi, J.; Gotoh, H.; Urushima, T.; Shoji, M. *Angew. Chem., Int. Ed*. **2006**, *45*, 958. (i) Font, D.; Jimeno, C.; Pericas, M. A. *Org. Lett*. **2006**, *8*, 4653. (j) Mase, N.; Watanabe, K.; Yoda, H.; Takabe, K.; Tanaka, F.; Barbas, C. F., III. *J. Am. Chem. Soc*. **2006**, *128*, 4966.

(11) (a) Sayer, J. M.; Jencks, W. P. *J. Am. Chem. Soc*. **1973**, *95*, 5637. (b) Rosenberg, S.; Silver, S. M.; Sayer, J. M.; Jencks, W. P. *J. Am. Chem. Soc*. **1974**, *96*, 7986. (c) Sayer, J. M.; Pinsky, B.; Schonbrunn, A.; Washtein, W. *J. Am. Chem. Soc*. **1974**, *96*, 7998. (d) Kayser, R. H.; Pollack, R. M. *J. Am. Chem. Soc*. **1977**, *99*, 3379. (e) Sayer, J. M.; Conlon, P. *J. Am. Chem. Soc.* **1980**, *102*, 3592. (f) Yamataka, H.; Nagase, S.; Ando, T.; Hanafusa, T. *J. Am. Chem. Soc*. **1986**, *108*, 601. (g) Pliego, J. R., Jr.; Alcântara, A. F. C.; Veloso, D. P.; Almeida, W. B. *J. Braz. Chem. Soc*. **1999**, *10*, 381. (h) Mascavage, L. M.; Sonnet, P. E.; Dalton, D. R. *J. Org. Chem*. **2006**, *71*, 3435. (i) Evans, G. J. S.; White, K.; Platts, J. A.; Tomkinson, N. C. O. *Org. Biomol. Chem*. **2006**, *4*, 2616.

(12) (a) Williams, I. H.; Spangler, D.; Femec, D. A.; Maggiora, G. M.; Schowen, R. L. *J. Am. Chem. Soc.* **1983**, *105*, 31. (b) Williams, I. H.; Spangler, D.; Maggiora, G. M.; Schowen, R. L. *J. Am. Chem. Soc*. **1985**, *107*, 7717. (c) Williams, I. H. *J. Am. Chem. Soc*. **1987**, *109*, 6299. (d) Hall, N. E.; Smith, B. J. *J. Phys. Chem. A* **1998**, *102*, 4930.

(13) Some representative examples: (a) Andrey, O.; Alexakis, A.; Bernardinelli, G. *Org. Lett*. **2002**, *4*, 3611. (b) Halland, N.; Aburel, P. S.; Jørgensen, K. A. *Angew. Chem., Int. Ed*. **2003**, *42*, 661. (c) Melchiorre, P.; Jørgensen, K. A. *J. Org. Chem*. **2003**, *68*, 4151. (d) Andrey, O.; Alexakis, A.; Bernardinelli, G. *Org. Lett*. **2003**, *5*, 2559. (e) Halland, N.; Aburel, P. S.; Jørgensen, K. A. *Angew. Chem., Int. Ed*. **2003**, *42*, 661. (f) Betancort, J. M.; Sakthivel, K.; Thayumanavan, R.; Tanaka, F.; Barbas, C. F., III. *Synthesis* **2004**, 1509. (g) Mangion, I. K.; Northrup, A. B.; MacMillan, D. W. C. *Angew. Chem., Int. Ed*. **2004**, *43*, 6722. (h) Halland, N.; Aburel, P. S.; Jørgensen, K. A. *Angew. Chem., Int. Ed*. **2004**, *43*, 1272. (i) Cobb, A. J. A.; Shaw, D. M.; Longbottom, D. A.; Gold, J. A.; Ley, S. V. *Org. Biomol. Chem.* **2005**, *3*, 84. (j) Bartoli, G.; Bosco, M.; Carlone, A.; Cavalli, A.; Locatelli, M.; Mazzanti, A.; Ricci, P.; Sambri, L.; Melchiorre, P. *Angew. Chem., Int. Ed*. **2006**, *45*, 4966. (k) Wang, J.; Li, H.; Zu, L.; Jiang, W.; Xie, H.; Duan, W.; Wang, W. *J. Am. Chem. Soc*. **2006**, *128*, 12652.

(14) Water molecule released from the second step could facilitate an autocatalytic process.

of improved transition state stabilization as compared to an uncatalyzed pathway can result in noticeable reduction in the reaction time.

The density functional theory studies on proline-catalyzed direct aldol reaction between acetone and acetaldehyde by Boyd et al. highlighted the importance of proton transfer from the carboxylic acid group during enamine formation.[15] Moreover, it has been found that the enamine formation has barriers comparable to those of subsequent C−C bond formation, and hence it was thought that certain acid/base additives might be helpful in improving the overall rate of reaction by accelerating the enamine formation.[16] The use of additives (co-catalyst) has been frequently found in the literature albeit confined merely to experimental observation.[17] In a very recent study, Gellman et al. have efficiently employed variants of catechol as co-catalyst in organocatalyzed Michael reactions.[18] Since the co-catalyst was able to reduce the reaction time, it was proposed that the co-catalyst could be involved in activating the reactants through hydrogen bonding. However, explicit details on the role of co-catalysts on enamine formation are not available in the literature. Better insights on the effect of co-catalysts in promoting enamine formation will help improve the reaction conditions in the burgeoning area of enamine-mediated organocatalysis. As part of the ongoing research in organocatalyzed reactions,[19] we have initiated a detailed theoretical study using the ab initio and DFT methods toward understanding the enamine formation under neat conditions or with the inclusion of a co-catalyst. This study assumes additional relevance in the context of the overwhelming current interest in aqueous organocatalysis.[20] The results obtained by considering various modes through which a co-catalyst or reagent can help stabilize the transition states leading to enamines (under neat conditions or in the presence of added co-catalyst) are described in the following sections.

Computational Methods

All the transition state structures and reactants were fully optimized, first in the gas phase at (i) mPW1PW91/6-31G*, (ii) mPW1PW91/6-311+G**,[21] and (iii) MP2(full)/6-31G*[22] levels of theories using the Gaussian98 and Gaussian03 suite of quantum chemical programs.[23] The choice of these theoretical models is based on the available reports on the performance of various DFT functionals as well as to account for the likely long-range dispersive interactions in many of the transition states (vide infra). The energetics obtained with the correlated ab initio method using the MP2(full) level can capture the effects of dispersive interaction unlike the popular density functionals.[24] Among the commonly employed DFT functionals, mPW1PW91 has been known to perform relatively better with hydrogen-bonded systems.[25] Since the present work revolves around hydrogen bonding interactions at the transition states, we have employed a triple-ζ quality basis set including polarization functions on the hydrogen atoms along with diffuse functions on all the non-hydrogen atoms. Use of such augmented basis sets is recommended for improved performance of DFT methods.[26]

Both active- and passive-assisted pathways for the addition as well as the dehydration steps were considered with the explicit inclusion of reactant or co-catalyst molecules in the transition states (vide infra). This approach will enable the inclusion of specific solute−solvent interactions, such as the hydrogen bonding. Further, the gas-phase geometries were reoptimized at the $PCM_{(THF)}$/mPW1PW91/6-31G* level of theory using Tomasi's polarized continuum model (PCM).[27] The solvation energies are more sensitive to the structure and the electron density distribution. An appropriate theoretical model in conjunction with quality basis sets

(15) While a comprehensive experimental investigation on the kinetics of the key steps in organocatalyzed reactions is not available, the density functional theory studies by Boyd and co-workers have shown that the enamine formation between proline and acetone has comparable or even higher barriers in the gas phase than the ensuing C−C bond formation step. See: Rankin, K. N.; Gauld, J. W.; Boyd, R. J. *J. Phys. Chem. A* **2002**, *106*, 5155.

(16) (a) Tanaka, F.; Thayumanavan, R.; Mase, N.; Barbas, C. F., III. *Tetrahedron Lett.* **2004**, *45*, 325. (b) Pihko, P. M.; Laurikainen, K. M.; Usano, A.; Nyberg, A. I.; Kaavi, J. A. *Tetrahedron* **2006**, *62*, 317.

(17) (a) Austin, J.; MacMillan, D. W. C. *J. Am. Chem. Soc.* **2002**, *124*, 1172. (b) Mase, N.; Thayumanavan, R.; Tanaka, F.; Barbas, C. F. III. *Org. Lett.* **2004**, *6*, 2527. (c) Bertelsen, S.; Marigo, M.; Brandes, S.; Dinér, P.; Jørgensen, K. A. *J. Am. Chem. Soc.* **2006**, *128*, 12973. (d) Wang, W.; Li, H.; Wang, J.; Zu, L. *J. Am. Chem. Soc.* **2006**, *128*, 10354. (e) Menche, D.; Hassfeld, J.; Li, J.; Menche, G.; Ritter, A.; Rudolph, S. *Org. Lett.* **2006**, *8*, 741.

(18) (a) Chi, Y.; Gellman, S. M. *Org. Lett.* **2005**, *7*, 4253−4256. (b) Peelen, T. J.; Chi, Y.; Gellman, S. M. *J. Am. Chem. Soc.* **2005**, *127*, 11598.

(19) Shinisha, C. B.; Sunoj, R. B. *Org. Biomol. Chem.* **2007**, *5*, 1287.

(20) (a) Hayashi, Y. *Angew. Chem., Int. Ed.* **2006**, *45*, 8103. (b) Brogan, A. P.; Dickerson, T. J.; Janda, K. D. *Angew. Chem., Int. Ed.* **2006**, *45*, 8100. (c) Chen, X.-H.; Luo, S. W.; Tang, Z.; Cun, L.-F.; Mi, A.-Q.; Jiang, Y. Z.; Gong, L.-Z. *Chem.—Eur. J.* **2007**, *13*, 689. (d) Cao, Y.; Lai, Y.; Wang, X.; Lia, Y.; Xiaoa, W. *Tetrahedron Lett.* **2007**, *48*, 21.

(21) (a) Perdew, J. P.; Chevary, S. H.; Vosko, K. A.; Jackson, K. A.; Pederson, M. R.; Singh, D. J.; Fiolhais, C. *Phys. Rev. B* **1992**, *46*. (b) Perdew, J. P.; Chevary, S. H.; Vosko, K. A.; Jackson, K. A.; Pederson, M. R.; Singh, D. J.; Fiolhais, C. *Phys. Rev. B* **1993**, *48*. (c) Perdew, J. P.; Burke, K.; Wang, Y. *Phys. Rev. B* **1996**, *54*, 16533. (d) Adamo, C.; Barone, V. *J. Chem. Phys.* **1998**, *108*, 664.

(22) (a) Head-Gordon, M.; Pople, J. A.; Frisch, M. J. *Chem. Phys. Lett.* **1988**, *153*, 503. (b) Frisch, M. J.; Head-Gordon, M.; Pople, J. A. *Chem. Phys. Lett.* **1990**, *166*, 275. (c) Frisch, M. J.; Head-Gordon, M.; Pople, J. A. *Chem. Phys. Lett.* **1990**, *166*, 281.

(23) (a) Frisch, M. J.; Trucks, G. W.; Schlegel, H. B.; Scuseria, G. E.; Robb, M. A.; Cheeseman, J. R.; Zakrzewski, V. G.; Montgomery, J. A., Jr.; Stratmann, R. E.; Burant, J. C.; Dapprich, S.; Millam, J. M.; Daniels, A. D.; Kudin, K. N.; Strain, M. C.; Farkas, O.; Tomasi, J.; Barone, V.; Cossi, M.; Cammi, R.; Mennucci, B.; Pomelli, C.; Adamo, C.; Clifford, S.; Ochterski, J.; Petersson, G. A.; Ayala, P. Y.; Cui, Q.; Morokuma, K.; Malick, D. K.; Rabuck, A. D.; Raghavachari, K.; Foresman, J. B.; Cioslowski, J.; Ortiz, J. V.; Stefanov, B. B.; Liu, G.; Liashenko, A.; Piskorz, P.; Komaromi, I.; Gomperts, R.; Martin, R. L.; Fox, D. J.; Keith, T.; Al-Laham, M. A.; Peng, C. Y.; Nanayakkara, A.; Gonzalez, C.; Challacombe, M.; Gill, P. M. W.; Johnson, B. G.; Chen, W.; Wong, M. W.; Andres, J. L.; Head-Gordon, M.; Replogle, E. S.; Pople, J. A. *Gaussian 98*, revision A.11.4; Gaussian Inc.: Pittsburgh, PA, 2001. (b) Frisch, M. J.; Trucks, G. W.; Schlegel, H. B.; Scuseria, G. E.; Robb, M. A.; Cheeseman, J. R.; Montgomery, J. A., Jr.; Vreven, T.; Kudin, K. N.; Burant, J. C.; Millam, J. M.; Iyengar, S. S.; Tomasi, J.; Barone, V.; Mennucci, B.; Cossi, M.; Scalmani, G.; Rega, N.; Petersson, G. A.; Nakatsuji, H.; Hada, M.; Ehara, M.; Toyota, K.; Fukuda, R.; Hasegawa, J.; Ishida, M.; Nakajima, T.; Honda, Y.; Kitao, O.; Nakai, H.; Klene, M.; Li, X.; Knox, J. E.; Hratchian, H. P.; Cross, J. B.; Bakken, V.; Adamo, C.; Jaramillo, J.; Gomperts, R.; Stratmann, R. E.; Yazyev, O.; Austin, A. J.; Cammi, R.; Pomelli, C.; Ochterski, J. W.; Ayala, P. Y.; Morokuma, K.; Voth, G. A.; Salvador, P.; Dannenberg, J. J.; Zakrzewski, V. G.; Dapprich, S.; Daniels, A. D.; Strain, M. C.; Farkas, O.; Malick, D. K.; Rabuck, A. D.; Raghavachari, K.; Foresman, J. B.; Ortiz, J. V.; Cui, Q.; Baboul, A. G.; Clifford, S.; Cioslowski, J.; Stefanov, B. B.; Liu, G.; Liashenko, A.; Piskorz, P.; Komaromi, I.; Martin, R. L.; Fox, D. J.; Keith, T.; Al-Laham, M. A.; Peng, C. Y.; Nanayakkara, A.; Challacombe, M.; Gill, P. M. W.; Johnson, B.; Chen, W.; Wong, M. W.; Gonzalez, C.; Pople, J. A. *Gaussian 03*, revision C.02; Gaussian Inc.: Wallingford, CT, 2004.

(24) Šeèkutè, J.; Menke, J. L.; Emnett, R. J.; Patterson, E. V.; Cramer, C. J. *J. Org. Chem.* **2005**, *70*, 8649.

(25) (a) Pelekh, A.; Carr, R. W. *J. Phys. Chem. A* **2001**, *105*, 4697. (b) Porembski, M.; Weisshaar, J. C. *J. Phys. Chem. A* **2001**, *105*, 6655. (c) Klein, R. A.; Mennucci, B.; Tomasi, J. *J. Phys. Chem. A* **2004**, *108*, 5851. (d) Klein, R. A.; Zottala, M. A. *Chem. Phys. Lett.* **2006**, *419*, 254. (e) Matsuda, S P. T.; Wilson, W. K.; Xiong, Q. *Org. Biomol. Chem.* **2006**, *4*, 530.

(26) Lynch, B. J.; Zhao, Y.; Truhlar, D. G. *J. Phys. Chem. A* **2003**, *107*, 1384.

(27) (a) Cossi, M.; Barone, V.; Cammi, R.; Tomasi, J. *Chem. Phys. Lett.* **1996**, *255*, 327. (b) Cances, E.; Mennucci, B.; Tomasi, J. *J. Chem. Phys.* **1997**, *107*, 3032.

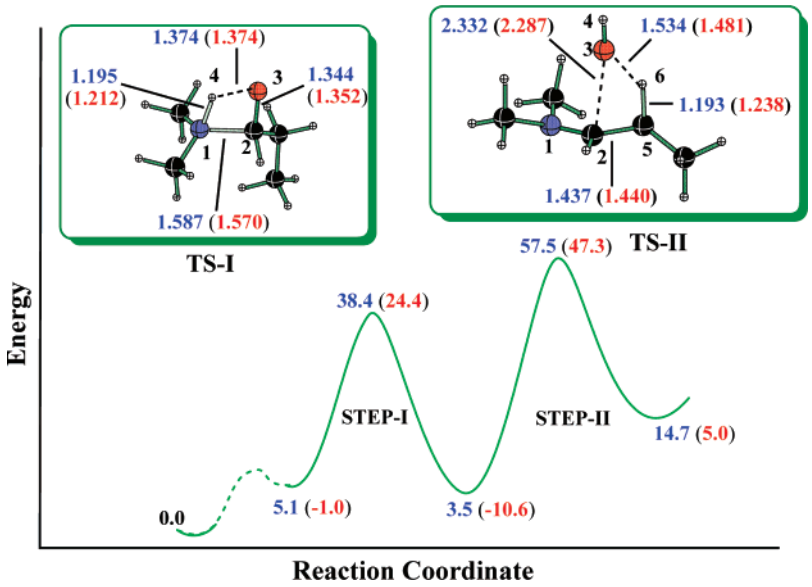

FIGURE 1. Reaction profile for enamine formation between dimethylamine and propanal computed at the mPW1PW91/6-31G* level of theory. Values in parentheses refer to the $PCM_{(THF)}$/mPW1PW91/6-31G* level of theory. Distances are in Å [atom colors: black = C, red = O, blue = N].

should therefore be good enough to obtain reasonably accurate estimates of solvation.[28] Thus, the treatment of both the continuum effects of solvent through an implicit model as well as the solute−solvent interactions through the explicit consideration of such interactions was included in the present study. This is reminiscent of a "discrete-continuum" model applied to a number of interesting reactions. In the present context, we are addressing the role of co-catalysts in the reaction between dimethylamine and propanal under *neat conditions*, where only small quantities of the co-catalyst are introduced as an additive.

The optimized geometries were characterized as stationary points on the potential energy surface at respective levels of theory by evaluating the vibrational frequencies. The transition states were characterized by one and only one imaginary frequency. These frequencies were identified to represent the correct reaction coordinate. Further, we have carried out 10% displacement on the transition state geometry along the direction of the imaginary vibrational frequency and subsequently reoptimized the perturbed structure using the "calcfc" option available in the program. This was to ensure whether the transition state is genuine and connects reactants and product. The intrinsic reaction coordinate (IRC) calculations were carried out at the mPW1PW91/6-311+G** as well as the B3LYP/6-311+G** levels of theory to further authenticate the transition states.[29]

In most cases involving the ancillary reagent (co-catalyst), a network of hydrogen bonding interactions is expected both in the transition states as well as near the entrance and exit channels for the addition and the dehydration steps. To understand the subtle electronic features of the kinetically significant transition states and intermediates, we have carried out topological analysis of electron density with the atoms in molecule (AIM) formalism using the wave functions obtained at the MP2/6-311+G** level on the MP2/6-31G* geometries of the transition states. The geometries for the prereacting complex clusters (toward the reactant as well as the product) are in most cases obtained at the mPW1PW91/6-311+G** level. These calculations were carried out with the AIM 2000 program.[30]

(28) Wiberg, K. B.; Rush, D. J. *J. Am. Chem. Soc.* **2001**, *123*, 2038.
(29) (a) Gonzalez, C.; Schlegel, H. B. *J. Chem. Phys.* **1989**, *90*, 2154. (b) Gonzalez, C.; Schlegel, H. B. *J. Phys. Chem.* **1990**, *94*, 5523.

Results and Discussion

We have investigated the reaction between dimethylamine and propanal leading to the corresponding enamine through a two-step pathway using the ab initio MP2 as well as DFT methods. While the first step involves the addition and simultaneous proton transfer resulting in a carbinolamine intermediate, the second step dehydration yields the product. On the basis of the mechanistic features, enamine formation pathways are organized into three models. First is an unassisted pathway, where the amine directly adds on to the electrophilic carbonyl group, as shown in Figure 1. In the second model, transition state stabilization via *passive* participation of reagent/co-catalyst is considered (vide infra). An *active* participation by reagent/co-catalyst forms the genesis of the third model. These models are constructed by explicit inclusion of reagent/co-catalyst in the respective transition states along the reaction pathway. The geometries of these transition states are further optimized in a dielectric continuum using the polarized continuum model (PCM) with the self-consistent reaction field (SCRF) method. The approach can be compared with the discrete-continuum methods employed for improved treatments of individual solute−solvent interactions.[31] The choice of methanol as the co-catalyst in this work is guided by the available experimental reports on the role of alcohol in promoting enamine formation under neat conditions.[18]

The activation barrier for the direct addition of amine to the carbonyl group is found to be fairly high.[32] The high gas-phase

(30) (a) Bader, R. F. W. *Atoms in Molecules: A Quantum Theory*; Clarendon Press: Oxford, 1990. (b) *AIM2000*, version 2.0; The Buro fur Innovative Software, SBK-Software, Bielefeld, Germany.
(31) (a) Claverie, P.; Daudey, J. P.; Langlet, J.; Pullman, B.; Piazzola, D.; Duron, M. *J. Phys. Chem.* **1978**, *82*, 405. (b) Pliego, J. R., Jr.; Riveros, J. M. *J. Phys. Chem. A* **2001**, *105*, 7241. (c) Cao, Z.; Lin, M.; Zhang, Q.; Mo, Y. *J. Phys. Chem. A* **2004**, *108*, 4277. (d) Balta, B.; Monard, G.; Ruiz-Lopez, M. F.; Antonie, M.; Gand, A.; Boschi-Muller, S.; Branlant, G. *J. Phys. Chem. A* **2006**, *110*, 7628. (e) Aikens, C. M.; Gordon, M. S. *J. Am. Chem. Soc.* **2006**, *126*, 12635.
(32) This prediction is in good concurrence with earlier examples reported by Boyd and others. Also see refs 11g, 11h, 12, and 15.

TABLE 1. Computed Activation Barriers[a] for Step I Obtained at Different Levels of Theory[b] for the Formation of Carbinolamine Involving One Ancillary Species[c]

	$\Delta H^{\ddagger}$ in kcal mol^{-1}					$\Delta G^{\ddagger}$ in kcal mol^{-1}				
	TS-I	**TS-Ia**	**TS-Ib**	**TS-Ic**	**TS-Id**	**TS-I**	**TS-Ia**	**TS-Ib**	**TS-Ic**	**TS-Id**
L1[d]	24.6	14.2	8.9	2.8	−5.1	38.4	38.2	32.8	28.5	20.1
L2[d]	24.6	17.3	14.6	4.1	−0.8	38.4	40.7	37.5	29.8	24.3
L3[d]	24.1	15.6	8.5	0.0	−6.5	38.2	38.1	32.3	26.0	18.7
L4[d,e]	–	–	–	–	–	24.5	19.0	13.3	4.0	−4.2

[a] Barriers with respect to the separated reactants. [b] All energies refer to the optimized geometries at respective levels of theory. [c] **TS-I** does not have ancillary species. [d] *L1* = mPW1PW91/6-31G*; *L2* = mPW1PW91/6-311+G**; *L3* = MP2(full)/6-31G*; *L4* = PCM-mPW1PW91/6-31G*. [e] Activation energies in THF obtained using the PCM (polarized continuum model) solvation model and UAKS radii.

barriers can be attributed to the larger charge separation that accompanies the addition of amine to the carbonyl carbon. The predicted high barrier for the dehydration step and the ease at which enamines are typically generated under laboratory conditions evidently indicate that the involvement of a direct addition−dehydration mechanism, as shown in Figure 1, is much less likely.[33] Therefore, we reasoned that additional possibilities such as a reagent/co-catalyst-assisted mechanism might be operating. The reactants (dimethylamine or propanal) or the co-catalysts (methanol) could in principle offer transition state stabilization by explicit interactions and thereby help reduce the barriers associated with each step. Two key assisted enamine formation routes are thus considered. Depending on the kind of stabilization of the transition states by the reactants/co-catalyst (in general termed as *ancillary* species), these are broadly classified as *passive*- and *active*-assisted catalytic pathways. In the first case, charge stabilization through the *passive* participation by the ancillary species via monofunctional interaction with the transition state is studied. In such cases, no noticeable distortion to the reaction coordinate is expected. It should also be reckoned that the charge separation in the transition state for addition is obviously higher than the separated reactants. In the second scenario, an *active* participation by the explicitly included ancillary species at the transition state, promoting a relay mechanism, is envisaged. Changes in the reaction coordinate are more likely in this model. Interestingly, a proton relay mechanism mediated by water molecules has been proposed for the enamine formation under biological conditions.[5f] For the sake of improved clarity, the discussions are broadly divided in two sections, on the basis of kinetically significant steps such as addition and dehydration.

(a) Formation of Carbinolamine (Step I). First, the unassisted pathway without the inclusion of explicit co-catalyst is considered. It is noticed that the C−N bond formation and the proton transfer to the carbonyl oxygen occur simultaneously when the amine adds to the aldehyde to form the carbinolamine intermediate (step I, Figure 1). The four-membered transition state geometry provides an optimal proton transfer distance to the developing alkoxide at the expense of increased strain that contributes to the higher barrier for the initial addition step.[12] The transition vector is identified as predominantly related to the proton transfer process. The intrinsic reaction coordinate calculation confirms that the addition transition state connects to the carbinolamine toward the product side and to an amine−aldehyde hydrogen-bonded complex on the reactant side. Further, the electron density at the bond critical points along N_1-C_2 and O_3-H_4 bond paths obtained using the AIM analysis is found to be significant in **TS-I**, implying a concerted process.[34] In the next step, dehydration through a cyclic four-membered TS involving the hydrogen from the β-carbon and the hydroxyl group results in enamine.[35] The Gibbs free energies of activation for the unassisted step I (**TS-I**) are found to be, respectively, 34.9 and 38.4 kcal mol^{-1} at the MP2/6-311+G**//6-31G* and mPW1PW91/6-311+G**//6-311+G** levels of theory. The agreement between the computed barriers at the MP2 as well as the mPW1PW91 levels with the same basis set is found to be consistently good (Table 1). More importantly, it is noticed that the activation barriers computed using the $PCM_{(THF)}$/mPW1PW91/6-31G* level is lower by 14 kcal mol^{-1} than that obtained from the gas-phase calculations (L1 versus L4). The solvent effects included using the continuum model evidently provide noticeable stabilization to these transition states having significant charge separation.[36] Interestingly, all the geometrical parameters obtained through full optimization in the condensed phase are found to be nearly the same as that of the gas-phase values.

At this juncture, it is worth noting that the reactants or the co-catalyst could stabilize the developing alkoxide ion in the transition state. Two different approaches are therefore considered, where either the reactant or the co-catalyst offers stabilization through hydrogen bonding interaction with the alkoxide oxygen. The optimized transition state geometries for the dimethylamine-assisted (**TS-Ia**) as well as the methanol-assisted (**TS-Ib**) pathways are provided in Figure 2. The computed activation barriers summarized in Table 1 evidently convey that the barriers for carbinolamine formation through the passive-assisted pathways (**TS-Ia** and **TS-Ib**) are lower than those in the unassisted route (**TS-I**). While the activation enthalpies show larger reduction in barriers arising through the effective hydrogen bonding with the *external* amine (reagent) or methanol (co-catalyst), the Gibbs free energies reflect only modest changes as compared to the unassisted pathway. The trends are found to be the same at the MP2 as well as the mPW1PW91 levels of theory. The larger reduction in the enthalpic barrier offered by the ancillary methanol can be attributed to the better hydrogen bonding ability of the methanolic −OH group. The O_3-H_7

(33) Enamines are normally generated in situ by stirring a carbonyl compound and amine in conventional organic solvents. Suitable electrophiles are subsequently provided in a one-pot strategy.

(34) (a) Summary of AIM analysis is provided in Table S1 in the Supporting Information. (b) See the Computational Methods for further details on the AIM calculation.

(35) In the case of carbinolamine generated from a primary amine, dehydration would result in an iminium ion (via step II). In absence of amino proton, as in the present case (secondary amine), the resulting product will be an enamine.

(36) (a) These results refer to the full geometry optimization within the continuum solvation model. (b) Additional calculations (using methanol as the solvent) at the $PCM_{(Methanol)}$/mPW1PW91/6-31G* level revealed that the barriers for initial addition and subsequent dehydration are, respectively, 24.4 and 45.5 kcal mol^{-1} as compared to the corresponding values obtained at the $PCM_{(THF)}$/mPW1PW91/6-31G* level (24.4 and 47.3 kcal mol^{-1}, respectively).

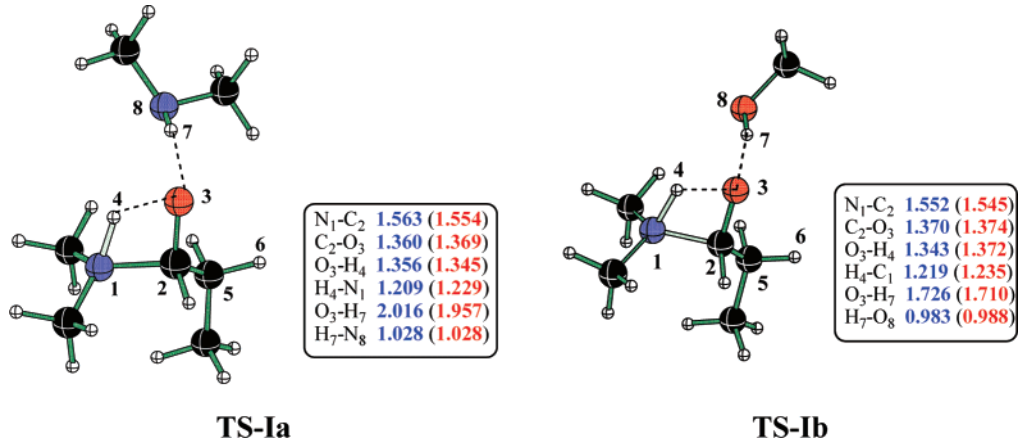

FIGURE 2. The mPW1PW91/6-311+G** optimized transition state geometries for step I with passive stabilization by dimethylamine (**TS-Ia**) and methanol (**TS-Ib**). Values in parentheses refer to the optimized bond lengths at the $PCM_{(THF)}$/mPW1PW91/6-31G* level of theory. Distances are in Å [atom colors: black = C, red = O, blue = N].

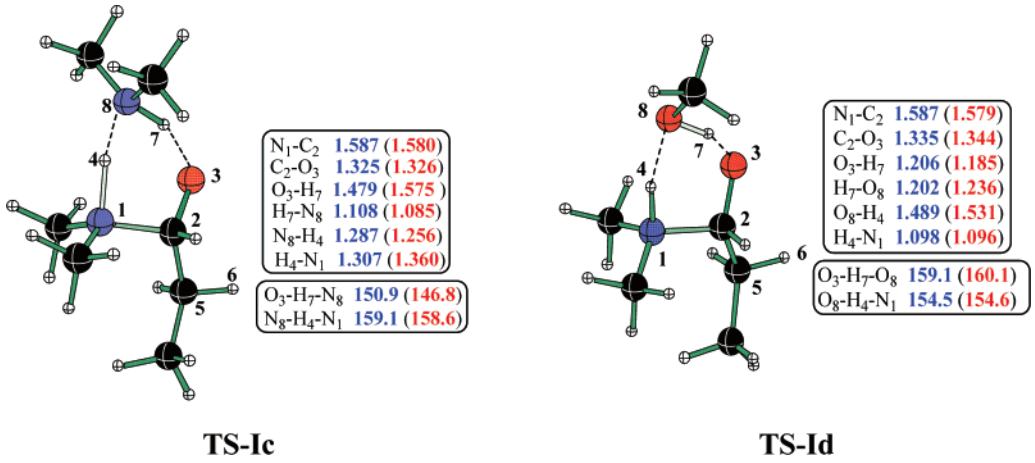

FIGURE 3. The mPW1PW91/6-311+G** optimized transition state geometries for step I with active-assisted pathway involving dimethylamine (**TS-Ic**) and methanol (**TS-Id**). Values in parentheses refer to the optimized geometrical parameters at the $PCM_{(THF)}$/mPW1PW91/6-31G* level of theory. Distances are in Å and angles in are in deg [atom colors: black = C, red = O, blue = N].

distance in **TS-Ib** is much shorter than that in **TS-Ia**, indicating a stronger interaction in the former case.[37] The energetics obtained through geometry optimization of the above transition states using the continuum solvation model are also found to exhibit similar trends as that predicted using the gas-phase calculations.

In the second model, as depicted in Figure 3, the possibility of *active* participation by one of the reagents or the co-catalyst in the transition state is considered. Here, the proton transfer to the developing alkoxide ion is not direct; instead, it is facilitated through dimethylamine or methanol via a relay mechanism. The stabilization of **TS-Ic** and **TS-Id** through a cyclic hydrogen-bonded network appears to be very effective. The computed addition barriers with this model are lower by about 20 and 29 kcal mol^{-1} ($PCM_{(THF)}$/mPW1PW91/6-31G* level), respectively, for the amine- and the methanol-assisted pathways, as compared to the unassisted pathways. This prediction is found to be consistently good at the mPW1PW91 as well as at the MP2 levels of theory. The key observation here pertains to the ability of the co-catalyst methanol (**TS-Id**) in promoting a relay proton transfer mechanism. Interestingly, the computed enthalpies of activation indicate that the explicit participation of methanol in this manner leads to a barrierless addition of the amine to the aldehyde. The negative activation energies predicted in this pathway arise from the use of separated reactants as the reference point (as zero) for the energy calculations. The barriers are found to be positive with respect to the respective prereacting complexes.[38] Nevertheless, for improved uniformity between various model transition state considered in this study, we have employed separated reactants as the reference point for calculating the activation barriers. The primary reason for such large reduction in barrier as compared to the unassisted or the passive-assisted pathways originates from the effective charge stabilization of the developing alkoxide oxygen through hydrogen

(37) (a) Changes in the hydrogen bonding abilities of dimethylamine and methanol are quite expected. Experimental pK_a values for Me_2NH and MeOH are, respectively, found to be 10.7 and 15.5 under aqueous conditions at 25 °C. (b) Perin, D. D. *Dissociation Constants of Organic Bases in Aqueous Solution*; Butterworths: London, 1965; Supplement, 1972. (c) Ben-Naim, A. *Solvation Thermodynamics*; Plenum Press: New York, 1987.

(38) As a representative case, the prereacting complexes are identified at the mPW1PW91/6-311+G** level of theory. The lower energy regions of the PES, near the entrance or the exit channels, could have many such weakly interacting PRCs, wherein the stabilizing interactions are maximized. A full sampling of the conformational feature of the PRCs is not performed in this study. Details on various PRCs might help elucidate the catalytic ability of explicit ancillary molecules as considered in this study. See Table S51 in the Supporting Information for details on the PRC.

TABLE 2. Computed Activation Parameters[a] for Step I Obtained at Different Levels of Theory[b] for the Formation of Carbinolamine Involving Two Ancillary Species

	$\Delta H^{\ddagger}$ in kcal mol^{-1}				$\Delta G^{\ddagger}$ in kcal mol^{-1}			
	TS-Ie	**TS-If**	**TS-Ig**	**TS-Ih**	**TS-Ie**	**TS-If**	**TS-Ig**	**TS-Ih**
L1[c]	6.3	−1.9	−9.5	−23.5	39.7	30.9	27.8	10.9
L2[c]	12.0	4.1	−2.9	−16.6	44.6	35.3	33.8	18.9
L3[c]	2.8	−4.5	−14.5	−23.6	36.5	29.3	22.7	11.0
L4[c,d]	–	–	–	–	11.5	2.7	−5.6	−17.9

[a] Barriers with respect to separated reactants. [b] All energies refer to the optimized geometries at respective levels of theory. [c] *L1* = mPW1PW91/6-31G*; *L2* = mPW1PW91/6-311+G**; *L3* = MP2(full)/6-31G*; *L4* = PCM-mPW1PW91/6-31G*. [d] Activation energies in THF obtained using the PCM (Polarized Continuum Model) solvation model and UAKS radii.

bonding interaction, besides the involvement of a less strained cyclic six-membered transition state. The efficiency of the former stabilizing effect is expected to vary from amine to alcohol. Evidently, based on the computed activation barriers, methanol is relatively more effective than dimethylamine in promoting the relay mechanism leading to the carbinolamine intermediate.

Examination of the geometric features of **TS-Ic** and **TS-Id** reveals that the proton transfer takes place in an asynchronous fashion (Figure 3). The N_1-H_4 bond in **TS-Ic** is considerably stretched, implying that the ancillary amine could accept a proton slightly ahead of transferring its proton to the developing alkoxide oxygen. Further, the imaginary normal mode of vibration is found to be predominantly related to the proton transfer process. When methanol acts as the co-catalyst, as in **TS-Id**, the H_7-O_8 bond is sufficiently elongated, suggesting that the proton transfer from the methanol is relatively ahead the proton abstraction from H_4-N_1. All these geometrical parameters remain nearly the same even after the inclusion of bulk solvent effects through the PCM model. Thus, it is to be anticipated that the assisted proton transfer mechanism could exhibit considerable sensitivity to the nature of ancillary species involved in transition state stabilization. This prediction has broader implications when the role of different additives on enamine formation is considered.[39]

As a logical extension of the transition state models considered in the present context, we became interested in investigating whether a second molecule of ancillary species could influence the reaction energetics. The role of a second ancillary species such as dimethylamine or methanol is therefore studied by precisely identifying the corresponding transition states, for the passive as well as the active modes of participation. The computed activation barriers associated with these transition state models are summarized in Table 2. In the case of the passive involvement, two ancillary species around the developing alkoxide oxygen offer additional Coulombic stabilization as shown in **TS-Ie** and **TS-If** (Figure 4). On the basis of the hydrogen bonding distances, it is evident that the stabilization by the methanol is relatively better than that offered by the dimethylamine. This indeed is reflected in the computed activation barriers for the passive-assisted pathways, where the reduction in barrier is much more pronounced in the case of methanol than with dimethylamine (Table 2). Further, the activation barriers for the initial nucleophilic addition in the passive-assisted pathway involving two molecules of the ancillary species are lower than the corresponding barriers computed for the single-molecule-assisted pathway. Notwithstanding the unfavorable entropic issues, improved transition state stabilization seems tangible when multiple ancillary species participate in the stabilization.[40] This observation clearly appears to be a useful starting point toward establishing the role of additives in organocatalytic reactions, where the rate-limiting step could be the generation of enamine/iminium intermediate, not the ensuing C−C bond formation.[15]

The optimized transition state geometries with the passive involvement of two ancillary species exhibited structural features similar to that of the unassisted pathway. The reaction coordinate continues to be dominated by the proton transfer from the amino nitrogen to the carbonyl oxygen. The critical N_1-C_2 bond distance is found to be shorter in the assisted pathway. For instance, the N_1-C_2 distances in **TS-Ie** and **TS-If** are, respectively, 1.55 and 1.54 Å, while that in the unassisted pathway is 1.59 Å (**TS−I**) at the mPW1PW91/6-311+G** level. Similar trend is also noticed for the proton transfer distances between N_1 and O_3 as evident from the O_3-H_4 bond distances (Figure 4). These geometrical features along with the electron densities at the bond critical points, $\rho(r_c)$, computed using the AIM formalism indicate that the transition states for the passive-assisted modes are more tightly bound as compared to the unassisted pathway. The bond critical points are also identified for the hydrogen bonding contacts between the developing alkoxide oxygen and the hydrogen(s) of the ancillary species.[41] It can be gleaned from the data provided in Table 2 that improved charge stabilization by the ancillary species evidently leads to effective lowering of the activation barrier for the addition of dimethylamine to propanal (step I).

Next, two ancillary species in the active mode of participation are considered. The transition states for the proton transfer through a cyclic relay mechanism are identified. The optimized geometries depicting the relay proton transfer involving dimethylamine as well as methanol are provided in Figure 5. The Gibbs free energy of activation is found to be lower than that of the other assisted as well as the unassisted pathways noted earlier. The barrier computed using the "cluster-continuum" method (the cluster inclusive of the addition transition state along with the explicit ancillary species embedded in a continuum THF dielectric using the PCM) interestingly indicates a barrierless addition when two methanol molecules participate in the active mode of stabilization (Table 2). The results clearly convey that the relay proton transfer mechanism is much more effective than the passive mode in carbinolamine formation between dimethylamine and propanal.

The optimized structural parameters of transition states **TS-Ig** and **TS-Ih** exhibit similar features as compared to the passive mode of stabilization. In the case of the amine-assisted pathway, the proton transfer from N_1 to N_{10} is found to be ahead of the proton abstraction by the carbonyl oxygen from the second amine molecule. In the methanol-assisted pathway, the proton transfer to the developing alkoxide ion by the second methanol takes place slightly ahead of the proton removal from the amino

(39) (a) It is worth taking note of the increasing current interest on the role of additives in improving organocatalytic reactions. (b) See refs 16 and 18.

(40) In an earlier study, Williams and co-workers have shown that potential energy terms are more suitable for discussion on the catalytic power of explicit solvents/ancillary species. See ref 12a. Since the focus of the present study is on the role of co-catalyst in reactions carried out under neat conditions, we believe that the free energy terms are more appropriate energy parameters for discussions.

(41) See Tables S1−S14 in Supporting Information for full list of AIM data.

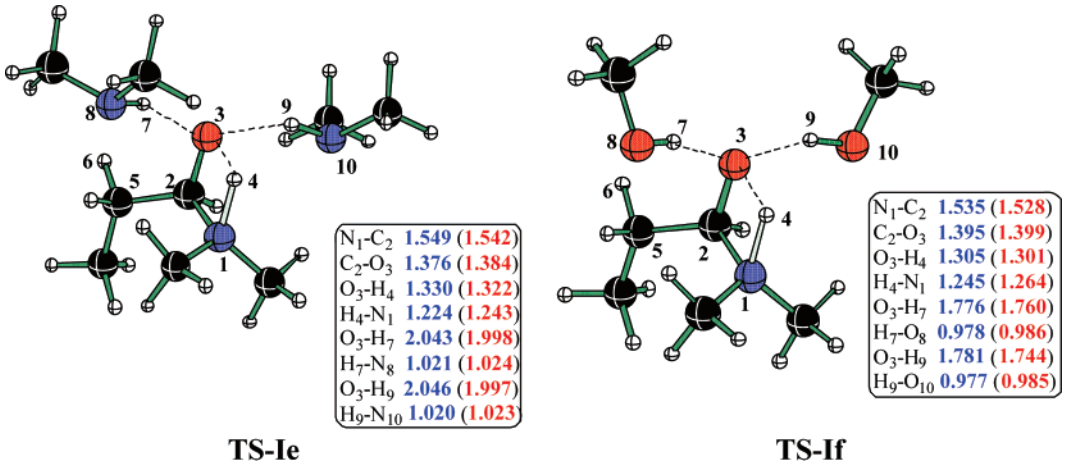

FIGURE 4. The mPW1PW91/6-311+G** transition state geometries for step I with passive stabilization by dimethylamine (**TS-Ie**) and methanol (**TS-If**). Values in parentheses refer to the optimized bond lengths at the $PCM_{(THF)}$/mPW1PW91/6-31G* level of theory. Distances are in Å [atom colors: black = C, red = O, blue = N].

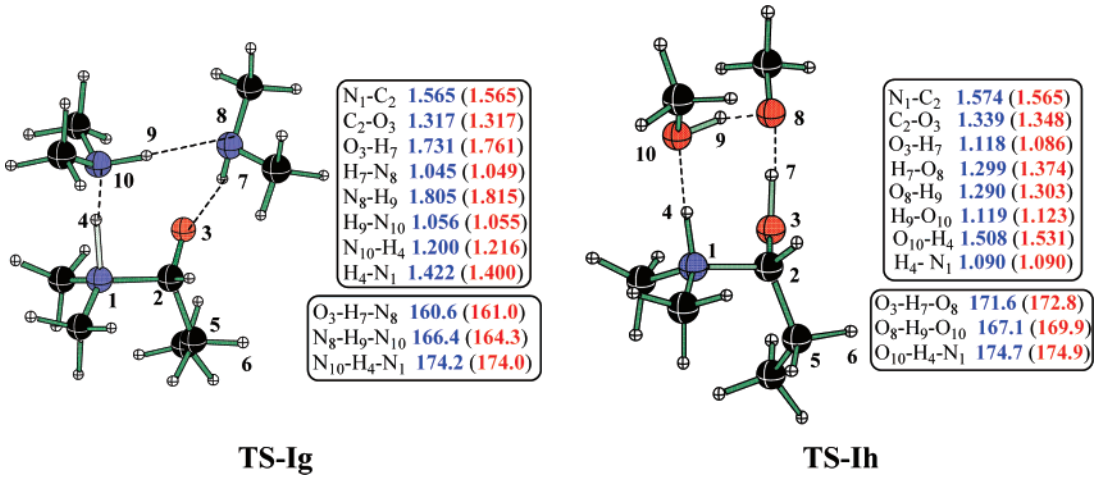

FIGURE 5. The mPW1PW91/6-311+G** transition state geometries for step I with active-assisted pathway by dimethylamine (**TS-Ig**) and methanol (**TS-Ih**). Values in parentheses refer to the optimized bond lengths at the $PCM_{(THF)}$/mPW1PW91/6-31G* level of theory.

nitrogen. Further, the geometrical details such as the linearity of the hydrogen bonding interactions (as revealed by N−H−N, N−H−O, N−H−O, and O−H−O bond angles along the cyclic loop and the corresponding distances) reveal that the proton transfer is effective in both **TS-Ig** and **TS-Ih**.[42] Interestingly, when a second ancillary species helps to facilitate the proton transfer, the linearity of the hydrogen bonding interactions is found to be better than when only one ancillary species is involved. For instance, in **TS-Ih**, $O_3-H_7-O_8$, $O_8-H_9-O_{10}$, and $O_{10}-H_4-N_1$ angles are, respectively, 171.6, 167.1, and 174.7°, whereas the corresponding angles in **TS-Id** are less than 160°.[43] The hydrogen-bonded network is further confirmed by identifying the corresponding bond critical points along the cyclic loop using the AIM formalism.[34] Such effective hydrogen bonding interactions will help reduce the likely strain associated with the cyclic relay proton transfer in these transition structures as compared to the unassisted pathway.

In the case of assisted pathways involving two ancillary species, additional configurations such as the hydrogen bonding interaction of a second ancillary species with the first, which itself is involved in active or passive stabilization, are considered. The optimized transition state geometries pertaining to these possibilities are provided in Figure 6. The transition states **TS-Ii** and **TS-Ij** represent a passive−passive mode of stabilization, respectively, for amine- as well as methanol-assisted addition steps. Comparison of the activation parameters for **TS-Ii** with that of **TS-Ie**, where two dimethylamine molecules directly interact with the developing alkoxide ion, exhibited little difference, implying that the passive−passive stabilizations are equally effective (Table 3). Similar trends are also noticed for the methanol-assisted passive−passive pathways (**TS-1f** versus **TS-Ij**).

The participation of two ancillary molecules in the active−passive mode, as depicted in **TS-Il** and **TS-Im** (Figure 6), is found to be enthalpically more favored over the corresponding situation when only one ancillary species is involved in the active mode of stabilization. The Gibbs free energy of activation obtained at the MP2 as well as at the PCM-mPW1PW91 levels implies that the participation of a second ancillary species can

(42) See Tables S21−S45 in Supporting Information for the complete list of optimized geometrical parameters for various transition states.

(43) In the case single methanol-assisted pathway as shown in **TS-Id**, $O_3-H_7-O_8$ and $O_8-H_7-N_1$ angles are found to be 159.1 and 154.5°, respectively.

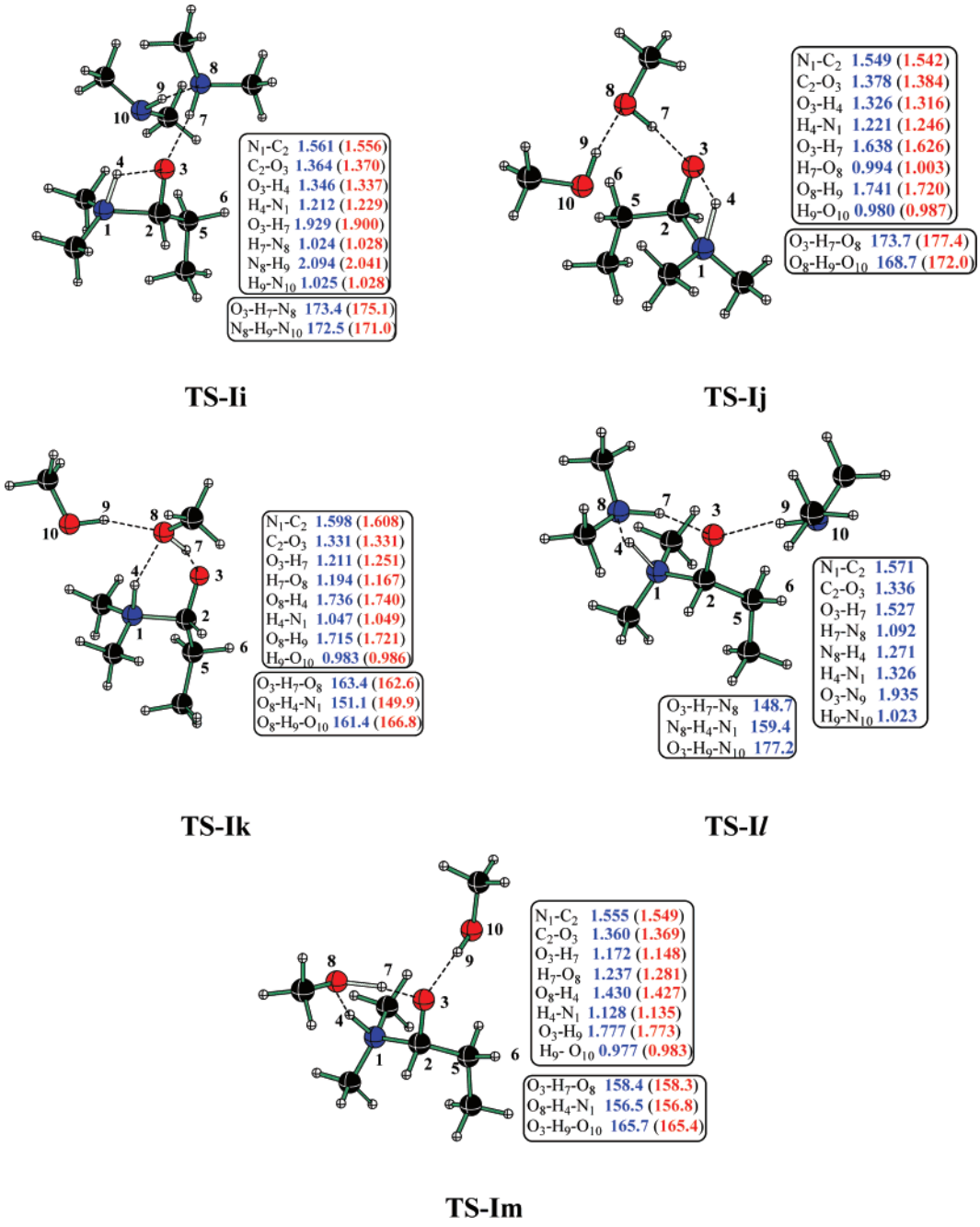

FIGURE 6. The mPW1PW91/6-311+G** transition state geometries for step I in the passive−passive- and the active−passive-assisted pathways by dimethylamine (**TS-Ii** and **TS-Il**) and methanol (**TS-Ij**, **TS-Ik**, and **TS-Im**). Values in parentheses refer to the optimized bond lengths at the $PCM_{(THF)}$/mPW1PW91/6-31G* level of theory.

offer additional transition state stabilization as compared to **TS-Ic** wherein only one molecule of dimethylamine participates in a relay hydrogen transfer mechanism facilitated by hydrogen bonding. The extent of stabilization is found to be more pronounced when methanol acts as the ancillary species (**TS-Ib** versus **TS-Ik**). These predictions evidently point to the importance of an active−passive transition state stabilization in the co-catalyst-assisted enamine formation. The most interesting aspect pertaining to the assisted pathway involving two ancillary methanol molecules evolves from the comparison of **TS-Ih** with **TS-Ik** as well as **TS-Im**. It is noticed that the cyclic proton relay mechanism through two methanol molecules in the active−active mode (**TS-Ih**) is distinctly more effective than the active−passive pathway (**TS-Ik**, **TS-Im**).

(b) Dehydration of Carbinolamine (Step II). The second major step toward the enamine formation is the dehydration of the carbinolamine intermediate generated in the first step. More importantly, this step is known to be the rate-limiting step of the reaction.[11g,h] The predicted activation barrier for unimolecular dehydration is found to be much higher than that of the addition step. For instance, the enthalpy and Gibbs free energies of activation for the unassisted pathway are, respectively, 34.5 and 46.7 kcal mol^{-1} at the mPW1PW91/6-311+G** level of theory.[44] The barriers are found to be even higher upon inclusion

TABLE 3. Computed Activation Parameters[a] for Step I Obtained at Different Levels of Theory[b] for the Formation of Carbinolamine Involving Two Ancillary Species through Passive−Passive and Active−Passive Modes of Stabilization

	$\Delta H^{\ddagger}$ in kcal mol^{-1}					$\Delta G^{\ddagger}$ in kcal mol^{-1}				
	TS-Ii	**TS-Ij**	**TS-Ik**	**TS-Il**	**TS-Im**	**TS-Ii**	**TS-Ij**	**TS-Ik**	**TS-Il**	**TS-Im**
L1[c]	7.2	−2.9	−18.8	−6.3	−17.1	40.2	30.6	15.2	27.8	17.4
L2[c]	11.5	2.5	−12.1	−0.9	−11.7	44.2	35.3	21.7	33.2	22.9
L3[c]	4.3	−4.1	−20.3	−8.6	−20.2	37.0	28.9	14.0	25.3	15.8
L4[c,d]	–	–	–	–	–	11.8	1.5	−15.0	−1.3[e]	−14.5

[a] Barriers with respect to separated reactants. [b] All energies refer to the optimized geometries at respective levels of theory. [c] *L1* = mPW1PW91/6-31G*; *L2* = mPW1PW91/6-311+G**; *L3* = MP2(full)/6-31G*; *L4* = PCM-mPW1PW91/6-31G*. [d] Activation energies in THF obtained using the PCM (Polarized Continuum Model) solvation model and UAKS radii. [e] Single-point energy computed at the PCM-mPW1PW91/6-31G*//mPW1PW91/6-31G* level of theory. In spite of repeated attempts in the condensed phase, **TS-Il** could not be located due to geometric convergence issues.

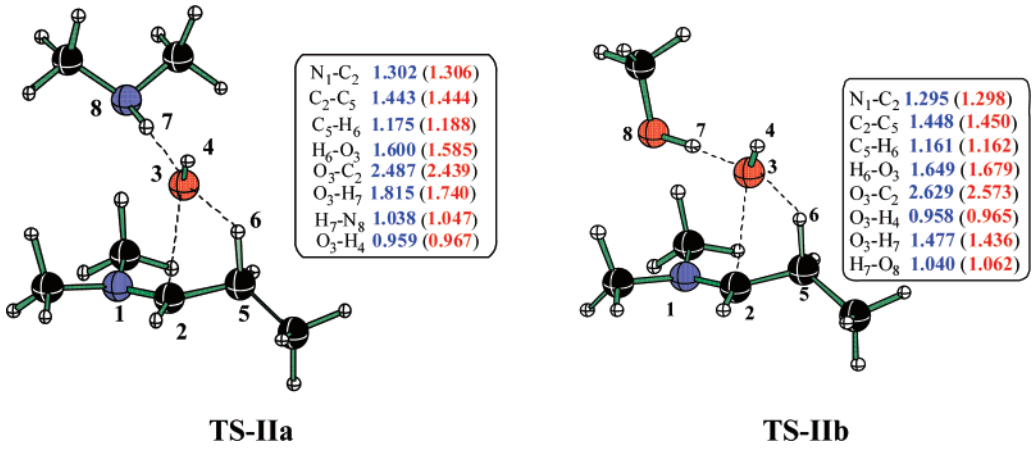

TS-IIa **TS-IIb**

FIGURE 7. The mPW1PW91/6-311+G** transition state geometries for step II with the passive-assisted pathway by dimethylamine (**TS-IIa**) and methanol (**TS-IIb**). Values in parentheses refer to the optimized bond lengths at the $PCM_{(THF)}$/mPW1PW91/6-31G* level of theory.

of solvent effects using the continuum model, evidently conveying that the studies directed toward understanding the rate enhancement in enamine formation should focus on the dehydration step rather than the initial addition step. In the following sections, we intend to summarize the key findings on the kinetically important dehydration step leading to enamine formation.

In the case of the unassisted dehydration pathway, the C_2-O_3 and C_5-H_6 bond cleavages proceed through a strained four-membered transition state. The poor leaving group ability of the OH^- combined with the C−H bond breaking results in a relatively higher barrier for the dehydration step as compared to the initial addition (**TS-II**, inset Figure 1). The C_2-O_3 distance in **TS-II** is quite elongated. The calculated bond indices as well as the electron density at the bond critical point for the C_2-O_3 bond are also found to be very low.[45] On the basis of these structural features and the imaginary normal mode of vibration pertaining to the reaction coordinate, it is identified that the dehydration transition state is predominantly related to the C_5 proton abstraction. Further, the extended IRC calculations confirm that **TS-II** connects to the carbinolamine and an enamine−H_2O complex, respectively, toward the reactant and product sides.

Akin to the addition step described earlier, four different transition state models are first conceived with one explicitly included ancillary species. In the passive mode of transition state stabilization, the hydrogen bonding between the developing charges and the ancillary species is noticed in the optimized geometries (Figure 7). The optimized transition state geometries for the passive-assisted modes, **TS-IIa** and **TS-IIb**, exhibit only a minor deviation with respect to the four-membered transition state earlier identified for the unassisted pathway (**TS-II**, Figure 1). The inclusion of long-range solvation effects through the continuum solvation model is found to bring about little variation on the gas-phase geometries. Since the rate-determining step in the enamine formation is the carbinolamine dehydration, the effect of ancillary stabilizing agents is expected to be more critical to the overall speed of the reaction. The computed activation barriers for different assisted transition state models are summarized in Table 4. The passive stabilization by dimethylamine (**TS-IIa**) as well as methanol (**TS-IIb**) is found to be effective in reducing the barrier when compared to the direct unimolecular dehydration. For instance, the activation barrier for the passive methanol-assisted dehydration is evidently lower than that in the unassisted pathway. The inclusion of diffuse functions on the MP2/6-31G* geometries by means of single-point energy calculations resulted in further reduction in the barrier by about 7 kcal mol^{-1} in the methanol-assisted pathway.[46] The computed energetics using the optimized geometries in the condensed phase (with THF as the continuum dielectric) also exhibit similar trends as predicted in the gas phase. It can also be noticed that the dehydration assisted by

(44) (a) The mPW1PW91/6-311+G** barrier is found to be in very good agreement with that obtained at the MP2 as well as CBS-QB3 levels. (b) See Tables S12 and S13 in Supporting Information.

(45) See Tables S9 and Figure S2 in the Supporting Information for AIM and bond order analyses for **TS-II**.

(46) (a) Computed barriers at the MP2(full)/6-311+G**//MP2(full)/6-31G* level of theory for steps I and II are tabulated in Tables S15−S20 in the Supporting Information. (b) The single-point energy calculations with the 6-311+G** basis sets are avoided within the PCM framework as the diffuse functions could lead to electron density tails outside the solute cavities generated by the molecularly shaped interlocking spheres.

TABLE 4. Computed Activation Barriers[a] for Step II Obtained at Different Levels of Theory[b] for the Dehydration Step Assisted by One Ancillary Species[c]

	$\Delta H^{\ddagger}$ in kcal mol^{-1}					$\Delta G^{\ddagger}$ in kcal mol^{-1}				
	TS-II	**TS-IIa**	**TS-IIb**	**TS-IIc**	**TS-IId**	**TS-II**	**TS-IIa**	**TS-IIb**	**TS-IIc**	**TS-IId**
L1[d]	44.8	31.3	21.6	34.9	20.7	57.5	54.0	44.2	58.1	43.9
L2[d]	34.5	25.6	16.0	27.8	15.3	46.7	47.8	38.5	50.9	37.4
L3[d]	47.7	33.4	20.6	37.5	19.4	60.3	56.0	43.6	60.6	42.1
L4[d,e]	–	–	–	–	–	47.2	36.3	26.8	39.4	21.2

[a] Barriers with respect to the separated reactants. [b] All energies refer to the optimized geometries at respective levels of theory. [c] **TS-II** does not have any ancillary species. [d] *L1* = mPW1PW91/6-31G*; *L2* = mPW1PW91/6-311+G**; *L3* = MP2(full)/6-31G*; *L4* = PCM-mPW1PW91/6-31G*. [e] Activation energies in THF obtained using the PCM (Polarized Continuum Model) solvation model and UAKS radii.

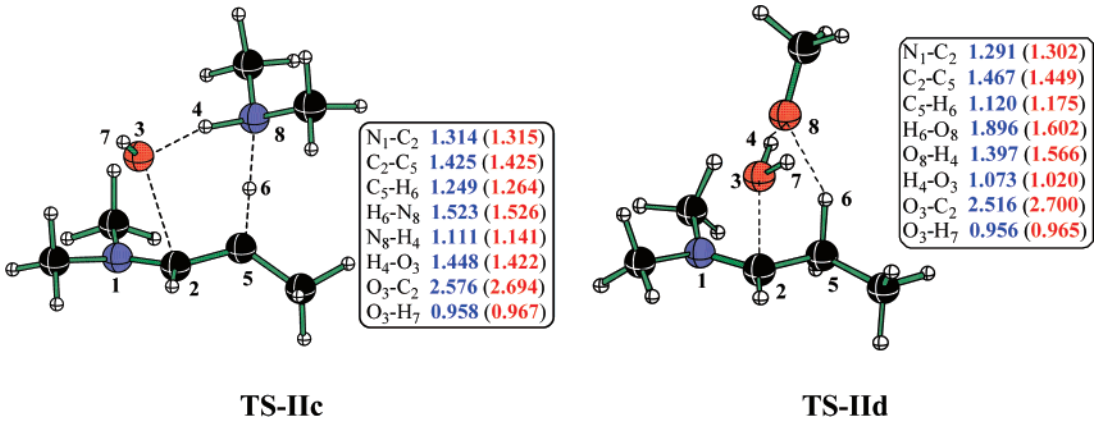

TS-IIc **TS-IId**

FIGURE 8. The mPW1PW91/6-311+G** transition state geometries for step II with the active-assisted pathway by dimethylamine (**TS-IIc**) and methanol (**TS-IId**). Values in parentheses refer to the optimized bond lengths at the $PCM_{(THF)}$/mPW1PW91/6-31G* level of theory.

dimethylamine is less effective as compared to methanol. On the basis of the computed activation barriers, it is evident that the co-catalyst-assisted dehydration is energetically more favored over the direct unassisted pathway.

In the active-assisted dehydration process, only methanol is found to be effective in rendering any significant stabilization to the transition state. When the relay proton transfer is promoted by methanol (**TS-IId**), the reduction in barrier is found to be about 9 kcal mol^{-1} as compared to that of the unassisted pathway at the mPW1PW91/6-311+G** level. A comparison between the computed activation barriers for the passive- and the active-assisted pathways by methanol suggests that they are equally effective in the dehydration step. This is at variance with the initial addition step (vide supra), where the active involvement of the ancillary species is found to be much more effective than the passive involvement. Whereas the reduction in strain associated with the four-membered transition state assumes greater importance in the latter case, the Coulombic stabilization of the departing −OH group by the ancillary species holds the key to the second step. It is therefore expected that the stabilization offered by the ancillary species in both the active and the passive modes is quite comparable in the second step. Another interesting point emerging from the data as given in Table 4 relates to the effect of higher basis sets in the dehydration step. The computed activation barriers are found to be lower with the triple-ζ quality basis set augmented with diffuse functions and additional polarization on hydrogen atoms.[47] The inclusion of bulk solvation effects through the continuum models in general predicts relatively lower barrier as compared to those in the gas-phase calculations.

The analysis of the transition vectors for the assisted pathways indicates that the proton transfer along a cyclic loop of hydrogen bonds dominates the reaction coordinate. The C_2-O_3 distances in all the transition states are considerably stretched (Figure 8).[42] Smith and co-workers have observed similar features with the transition states in water-assisted iminium ion formation.[12d] The geometrical features of the amine-assisted dehydration (**TS-IIc**) convey that the deprotonation is ahead of the −OH protonation (as indicated by the C_5-H_6 distance of 1.25 Å). The comparison of transition state structural parameters for the dehydration process via the assisted (**TS-IIc**, **TS-IId**) and the unassisted (**TS-II**) pathways reveals similar values for the C_2-O_3 distances. In the case of the methanol-assisted dehydration (**TS-IId**), the C_2-OH protonation takes place marginally ahead of the C_5-H_6 proton abstraction by the methanol, through a cyclic relay mechanism. In all these transition states, the optimized geometrical parameters, particularly, the C_2-O_3 and the C_5-H_6 bond distances, computed in the gas phase as well as in the THF dielectric continuum are found to be in good agreement. While the C_2-O_3 distances for the dehydration transition states are related in different models, the activation energies for the assisted pathways are much lower as compared to those in the unassisted pathway.

The largest reduction in barrier, when compared to the unassisted pathway, for the dehydration step is provided by the co-catalyst methanol. This prediction indicates that the explicit inclusion of additives (methanol) in the rate-limiting transition state could possibly account for the changes in reaction rates associated with the enamine formation. Similar observations relating to the importance of explicit solute−solvent interactions

(47) A reduction in barrier on the order of 5−7 kcal mol^{-1} is noticed at the mPW1PW91/6-311+G** (L2) level compared to mPW1PW91/6-31G*-(L1). The corresponding changes predicted at the MP2(full)/6-311+G**//MP2(full)/6-31G* level are found to be even larger and also conform with this trend.

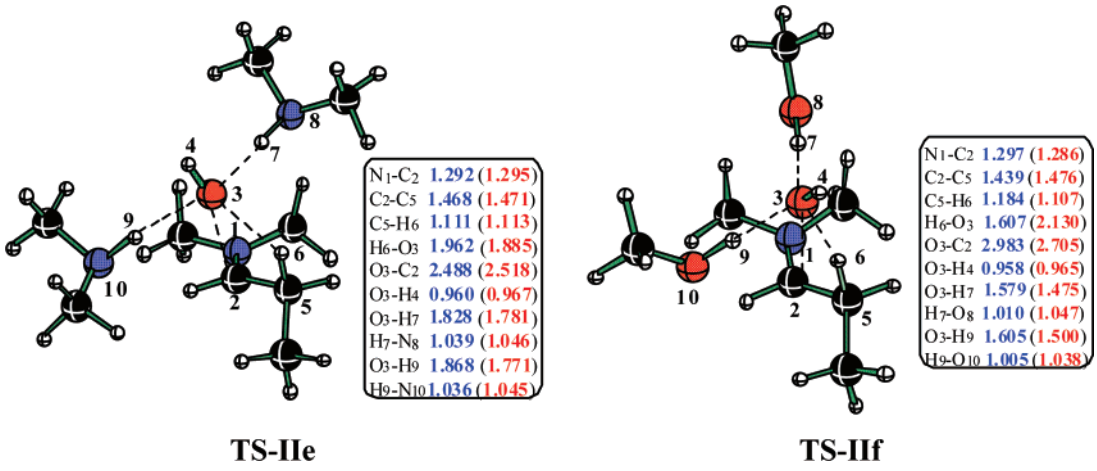

FIGURE 9. The mPW1PW91/6-311+G** transition state geometries for step II with the passive-assisted pathway by dimethylamine (**TS-IIe**) and methanol (**TS-IIf**). Values in parentheses refer to the optimized bond lengths at the $PCM_{(THF)}$/mPW1PW91/6-31G* level of theory.

TABLE 5. Computed Activation Barriers[a] for Step II Obtained at Different Levels of Theory[b] for the Dehydration Step Assisted by Two Ancillary Species[c]

	$\Delta H^{\ddagger}$ in kcal mol^{-1}				$\Delta G^{\ddagger}$ in kcal mol^{-1}			
	TS−IIe	**TS−IIf**	**TS−IIg**	**TS−IIIg**	**TS−IIe**	**TS−IIf**	**TS−IIg**	**TS−IIIg**
L1[d]	20.8	0.6	2.0	0.3	52.9	32.6	34.9	32.8
L2[d]	18.1	−0.4	0.0	0.4	49.8	31.1	32.9	33.0
L3[d]	16.8	0.2	−2.8	0.4	50.1	33.5	32.1	32.2
L4[c,d]	–	–	–	–	24.7	5.7	6.0[e]	7.5

[a] With respect to separated reactants. [b] All energies refer to the optimized geometries at respective levels of theory. [c] Activation energies in THF obtained using the PCM (Polarized Continuum Model) solvation model and UAKS radii. [d] *L1* = mPW1PW91/6-31G*; *L2* = mPW1PW91/6-311+G**; *L3* = MP2(full)/6-31G*; *L4* = PCM-mPW1PW91/6-31G*. [e] In spite of repeated attempts, **TS-IIg** continued to be a second-order saddle point with an additional weak imaginary frequency pertaining to the methyl rotation from the methanol fragment.

in achieving improved estimates on reaction barriers are available in the literature.[48]

As a natural extension of what has been hitherto considered, it is logical to anticipate that the explicit inclusion of more numbers of ancillary species could influence the energetics of the rate-determining step. The possible participation of two explicit molecules of the ancillary species in the dehydration step is therefore examined. The transition states for both passive- and active-assisted dehydration modes are precisely identified. In the passive mode of stabilization (Figure 9, **TS-IIe** and **TS-IIf**), the initial guess geometries for the transition states are generated in such a way that the unfavorable interaction between the carbinolamine methyl groups and the ancillary species is kept to a minimal level. In the active mode (**TS-IIg**), two ancillary species help to avoid the involvement of a strained four-membered transition state by facilitating a relay proton transfer process.[49] The inclusion of an additional ancillary species is found to be effective in further reducing the barrier in both passive as well as active modes (Table 5). The most valuable prediction pertains to the largest reduction in the activation barrier when two methanol molecules stabilize the dehydration transition state. For instance, the Gibbs free energy of activation in the gas phase for **TS-IIf** is found to be around 30 kcal mol^{-1} at the mPW1PW1/6-31G* level as opposed to other models where the barriers are found to be even higher than 50 kcal mol^{-1}. It is worth noting that the enthalpy of activation is effectively reduced while the Gibbs free energies continue to be on the higher side when amine acts as the ancillary species. Interestingly, the experimental evidence seemingly in support of this prediction is available in the form of enamine mediated reactions, where amine was used as an additive. Pihko et al. have demonstrated that additives such as triethylamine are ineffective in offering any rate enhancements in the overall enamine formation reaction between ketones and aromatic aldehydes.[16b]

The orientation of the ancillary species in various transition states, particularly, when two explicit ancillary molecules are incorporated, evidently conveys that the inclusion of more ancillary species will be harder to accomplish. For example, in **TS-IIe**, where two amines participate in the passive stabilization, they tend to stay as far away as possible to minimize the interaction with the methyl groups on the carbinolamine. Including one more ancillary species in the passive mode clearly appears to be much less favorable on steric grounds. Attempts toward locating the transition state for the dehydration step involving active participation by two amine molecules continued to be elusive.[50] Additionally, increasing entropic costs arising

(48) (a) Kong, S.; Evanseck, J. D. *J. Am. Chem. Soc.* **2000**, *122*, 10418. (b) Huang, Y.; Rawal, V. H. *J. Am. Chem. Soc.* **2002**, *124*, 9662. (c) Chandrasekhar, J.; Shariffskul, S.; Jorgensen, W. L. *J. Phys. Chem. B* **2002**, *106*, 8087. (d) Domingo, L. R.; Andrés, J. *J. Org. Chem.* **2003**, *68*, 8662. (e) Mujika, J. I.; Mercero, J. M.; Lopez, X. *J. Am. Chem. Soc.* **2005**, *127*, 4445. (f) Saettel, N. J.; Wiest, O. *Tetrahedron* **2006**, *62*, 6490. (g) Gordillo, R.; Dudding, T.; Anderson, C. D.; Houk, K. N. *Org. Lett.* **2007**, *9*, 501.

(49) In spite of repeated attempts, the desired transition state for dehydration involving two ancillary amines could not be located. The attempts were also repeated at different levels of theory both in the gas phase and with the continuum model.

(50) We have tried a number of initial geometries with different orientation of dimethylamine molecules at the different levels of theory. Efforts toward step-wise as well as concerted dehydration processes were also not successful.

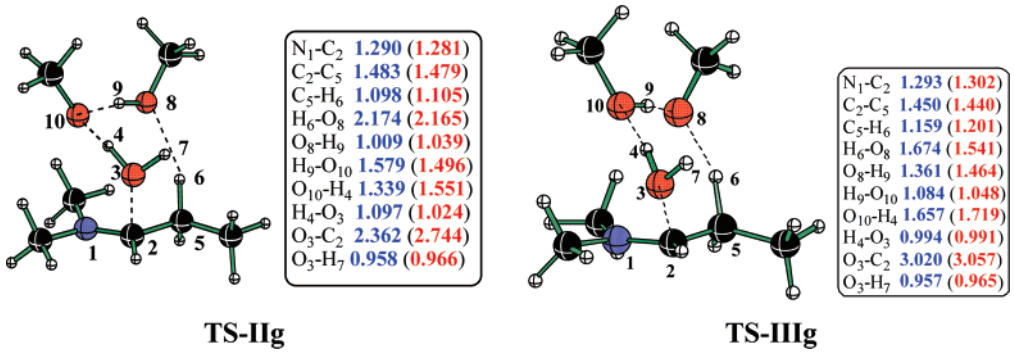

FIGURE 10. The mPW1PW91/6-311+G** transition state geometries for steps II and III exhibiting the active-assisted pathway by methanol (**TS-IIg** and **TS-IIIg**). Values in parentheses refer to the optimized bond lengths at the $PCM_{(THF)}$/mPW1PW91/6-31G* level of theory.

due to relatively larger compensation of translational as well as rotational degrees of freedom are expected to be important deterring factors in going beyond two ancillary species.

The optimized geometries of **TS-IIe**, **TS-IIf**, and **TS-IIg** provide additional details on the dehydration step. In this step, the C_2-O_3 bond cleavage is found to be quite advanced as compared to the C_5-H_6 distance in both the passive- and the active-assisted modes. The dehydration transition states are generally found to possess a considerably elongated C_2-O_3 bond (2.3 to 2.7 Å) with only negligible changes in the adjacent C_5-H_6 bond with respect to the preceding carbinolamine intermediate (reactant). Further, the $n_N \rightarrow \sigma^*(C_2-O_3)$ electron delocalizations in the carbinolamine intermediate calculated using the natural bond orbital (NBO) analysis are found to be significant.[51] The relatively higher population of $\sigma^*(C_2-O_3)$ can contribute toward a facile bond cleavage. To confirm whether **TS-IIf** and **TS-IIg** connect to the desired stationary points on either sides of the transition state, intrinsic reaction coordinate calculations (IRC) along the respective transition vectors are performed.[52] Interestingly, with the active methanol-assisted pathway through **TS-IIg**, the optimization toward the product side led to an iminium ion intermediate.[53] This evidently suggests the involvement of a two-step carbinolamine dehydration. First, the methanol-assisted removal of the −OH group leads to an iminium ion, which in turn yields the enamine upon abstraction of the C_5-H_6 proton, either by the hydroxide ion or by the ancillary species.[54]

The last step toward the generation of enamine from the iminium ion intermediate relates to the C_5-H_6 deprotonation. The transition state for the methanol-assisted deprotonation (**TS-IIIg**) is located. The imaginary frequency is found to possess characteristic features of a relay proton transfer, where one of the methanol molecules abstracts the C_5 proton and exchanges its proton with another molecule of methanol, as shown in Figure 10. The computed barrier associated with this step is provided in Table 5. Interestingly, the formation of enamine from iminium ion through step III has a barrier similar to that of the earlier step, that is, removal of −OH group (step II) assisted by two ancillary species (generation of iminium ion/methanol/water cluster from the carbinolamine). These predictions are quite valuable in light of the iminium ion catalysis proposed in a number of organocatalyzed reactions.[55] The formation of iminium ion from an aldehyde demands the removal of a poor leaving group such as the −OH.[17c] It is evident from the computed barriers that the participation of two ancillary methanol molecules could help remove the −OH group through a stabilized transition state. The methanol-assisted removal of the −OH group possesses a much lower barrier compared to the direct unimolecular elimination discussed earlier.

Two more transition state models for the dehydration step are identified with two molecules of dimethylamine (**TS-IIh**) or methanol (**TS-IIi**) as the ancillary species (Figure 11). In the first case, additional transition state stabilization by the second molecule of dimethylamine through hydrogen bonding is noticed. These models termed as the assisted passive−passive dehydration are found to be effective.[56] The additional enthalpic stabilization offered by a second molecule of dimethylamine is quite clear from the activation barriers for **TS-IIa** and **TS-IIh** (Table 6). In the case of methanol, the active−passive-assisted transition state (**TS-IIi**) is identified at the mPW1PW91/6-31G* level of theory both in the gas phase as well as in the condensed phase. On the basis of the activation barriers, albeit limited with regard to different levels of theories in the present case, it appears that the additional hydrogen bonding interaction through the active−passive mode can render further stabilization to the transition state.The high barrier for the unimolecular dehydration of carbinolamine together with the generation of enamines under neat conditions conspicuously points to the possible involvement of an assisted dehydration pathway. We have been able to delineate a number of possible models for the transition state stabilization for the reaction between dimethylamine and propanal leading to the corresponding enamine. These models

(51) Complete list of major delocalizations identified using the NBO analysis is summarized in Table S46 in the Supporting Information.

(52) (a) As these are nontrivial transition states, extended IRC calculations with 30 points each toward reactant and product have been carried out at both at the MP2/6-31G* and mPW1PW91/6-311+G** levels. The structural and energetic information obtained from the IRC calculations for **TS-IIg** (and **TS-IIIg**) is summarized in Table S47−S50 in the Supporting Information. (b) This analysis is supported by additional geometry optimizations using the "opt = calcfc" option on the perturbed geometries derived from the transition state by a 10% displacement along the reaction coordinate, on either side of the first-order saddle point. See Computational Methods for further details.

(53) We have taken additional care in establishing the existence of an intermediate along the reaction path. In this regard, the IRC runs have also been also performed at the MP2(full)/6-31G* level, in addition to that at the mPW1PW91/6-311+G** level. Search for iminium ion intermediate was not successful with all other transition state models considered for the dehydration step. See Table S48 in Supporting Information.

(54) See Figure S4 in the Supporting Information, where the geometry changes in along the IRC trajectory are provided.

(55) (a) Palomo, C.; Mielgo, A. *Angew. Chem., Int. Ed.* **2006**, *45*, 7876. (b) Enders, D.; Huttl, M. R. M.; Grondal, C.; Raabe, G. *Nature* **2006**, *441*, 861.

(56) The equivalent possibility with methanol (as in **TS-IIb**) could not be identified. Similarly, the inclusion of a second molecule of dimethylamine in the active mode (as in **TS-IIi**) was not possible due to severe steric crowding.

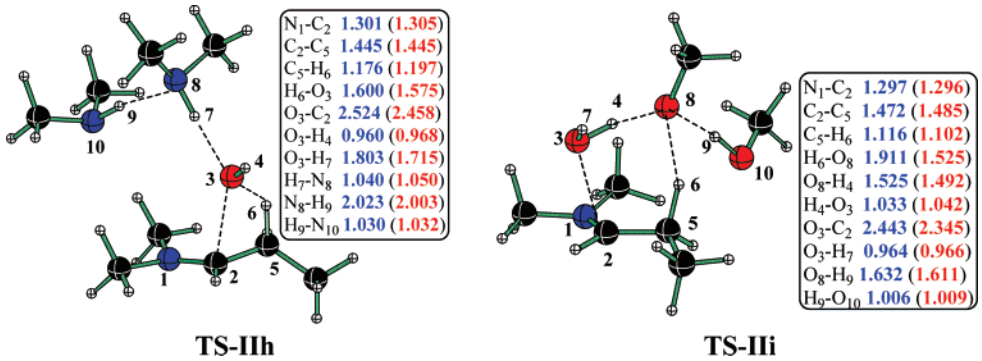

FIGURE 11. The mPW1PW91/6-311+G** transition state geometries for step II with the passive−passive-assisted pathway by dimethylamine (**TS-IIh**) and the mPW1PW91/6-31G* transition state geometry for step II for the active−passive-assisted pathway by methanol (**TS-IIi**). Values in parentheses refer to the optimized bond lengths at the $PCM_{(THF)}$/mPW1PW91/6-31G* level of theory.

TABLE 6. Computed Activation Barriers[a] for Step II Obtained at Different Levels of Theory for the Dehydration Step Assisted by Two Ancillary Species[b] (Passive−Passive and Active−Passive Combination)

	$\Delta H^{\ddagger}$ in kcal mol^{-1}		$\Delta G^{\ddagger}$ in kcal mol^{-1}	
	TS-IIh	**TS-IIi**	**TS-IIh**	**TS-IIi**
L1[c]	24.5	3.6	56.7	36.5
L2[c]	21.1	4.0[d]	51.5	36.5[d]
L3[c]	23.1	−0.4[e]	57.2	32.4[e]
L4[b,c]	−	−	30.9	6.4[f]

[a] With respect to the separated reactants. [b] Activation energies in THF obtained using the PCM (Polarized Continuum Model) solvation model and UAKS radii. [c] *L1* = mPW1PW91/6-31G*; *L2* = mPW1PW91/6-311+G**; *L3* = MP2(full)/6-31G*; *L4* = PCM-mPW1PW91/6-31G*. [d] Single-point energy at the mPW1PW91/6-311+G**//mPW1PW91/6-311G** level of theory. Attempts to locate **TS-IIi** were not successful even after repeated attempts. [e] Single-point energy at the MP2(full)/6-31G*//mPW1PW91/6-31G* level of theory. Thermal corrections to enthalpy and free energy are taken from the mPW1PW91/6-31G* level of theory. [f] **TS-IIi** continued to be a second-order saddle point with an additional imaginary frequency pertaining to the methyl rotation from the methanol fragment, even after several attempts.

successfully bring out the importance of the methanol-assisted pathways over the unassisted as well as the amine-assisted addition−dehydration process. These models serve as a good starting point toward identifying the critical role played by the co-catalysts and other additives in promoting enamine formation.[18] The increasing number of experimental studies aimed at exploiting the potential of organocatalytic reactions proceed through an enamine/iminium catalysis. Interestingly, the rate acceleration in such reactions could possibly rest with the ease of generation of enamine/iminium. We propose that one of the contributing factors to the observed rate acceleration in the presence of co-catalysts in the Michael reaction between enamine derived from proline analogues with methyl vinyl ketone could be the ease of generation of enamine.[18] While the predictions are based on chemically intuitive transition state models, one could anticipate alternative possibilities other than what is proposed herein.[57] Further, the absolute values of the predicted activation energies might show variations upon including higher-level electron correlation as well as with increasing the basis set size. We believe that the relative energies between different model pathways (direct, passive, as well as active-assisted pathways) will exhibit similar trends even at more accurate theoretical methods.[58]

Conclusion

The investigations on various possible pathways leading to the enamine formation by the reaction of a secondary amine with aldehyde, both in the presence and absence of explicit co-catalyst or one of the reagents, have been performed. The computed barriers, such as free energies as well as enthalpies of activation, unequivocally conveyed that the dehydration of carbinolamine is the rate-limiting step in this reaction. A number of transition state models involving active and passive participation of the ancillary molecules (methanol or dimethylamine) have been considered. It was found that a proton relay mechanism is energetically the most favored route for the formation of carbinolamine as well as for the subsequent dehydration leading to enamine. The efficiency of the proton transfer was found to be largely dependent on the nature of the ancillary species stabilizing the transition state. The overall catalytic ability of the co-catalysts was found to arise due to the improved transition state stabilization facilitated by effective hydrogen bonding.

Acknowledgment. Financial support from the Department of Science and Technology, New Delhi (through SR/S1/OC-50/2003), and computing facilities from IIT Bombay computer center are gratefully acknowledged. M.P. acknowledges CSIR-New Delhi for Senior Research Fellowship.

Supporting Information Available: The optimized geometries for all the stationary points obtained at different levels of theory, total electronic energies, bond order, natural charges (Figures S1 and S2), IRC plots (Figure S3 and S4), AIM analyses (Table S1 to S14), and of transition states are provided in electronic Supporting Information. This material is available free of charge via the Internet at http://pubs.acs.org.

JO071004Q

(57) An exhaustive sampling of the conformational space for possible prereacting complexes, wherein the stabilizing interactions are maximized, could be performed. Alternatively, a Monte-Carlo simulation might be of help (provided reliable potentials are available) toward improving the sampling. Such exercise could be challenging for the whole range of transition state models considered in the present study.

(58) A representative set of models was examined up to the complete basis set extrapolation limits using the CBS-QB3 level.[58a,b] See Tables S11−S13 in Supporting Information. Due to hardware limitations, we could not proceed with CBS-QB3 runs beyond systems having more than 9−10 heavy atoms. The agreement between the limited set of activation barriers obtained at the CBS-QB3 level and other theoretical models considered here is found to be quite good. (a) Montgomery, J. A., Jr.; Frisch, M. J.; Ochterski, J. W.; Petersson, G. A. *J. Chem. Phys.* **1999**, *110*, 2822. (b) Montgomery, J. A., Jr.; Frisch, M. J.; Ochterski, J. W.; Petersson, G. A. *J. Chem. Phys.* **2000**, *112*, 6532.